

FAST LEARNING FROM LABEL PROPORTIONS WITH SMALL BAGS

Denis Baručić, Jan Kybic

Department of Cybernetics, Faculty of Electrical Engineering, Czech Technical University in Prague

ABSTRACT

In learning from label proportions (LLP), the instances are grouped into bags, and the task is to learn an instance classifier given relative class proportions in training bags. LLP is useful when obtaining individual instance labels is impossible or costly.

In this work, we focus on the case of small bags, which allows designing more efficient algorithms by explicitly considering all consistent label combinations. In particular, we propose an EM algorithm alternating between optimizing a general neural network instance classifier and incorporating bag-level annotations. In comparison to existing deep LLP methods, our approach converges faster to a comparable or better solution. Several experiments were performed on two different datasets.

Index Terms— learning from label proportions, weak labels, deep learning

1. INTRODUCTION

Learning from label proportions (LLP) [1] is a case of a weakly supervised learning framework where the aim is to produce an instance classification model, knowing the proportions of class labels in groups of instances (*bags*) but not the individual instance labels.

The first applications of LLP were in modeling voting behavior from aggregated electoral district data, where individual data is not available because of privacy requirements. In *in vitro* fertilization (IVF), the task is to predict the likelihood of successful development of individual embryos [2] or oocytes [3], while the only hard data is the outcome of the pregnancy, which may have resulted from any of the several implanted embryos. In Langerhans islet detection [4], only subjective classification of individual objects is possible, while the total contents in the sample can be quantified by DNA content measurement. In counting applications, i.e., counting the number of people, animals, cells, cars, or other objects in the image [5], it is often cheaper to obtain the counts than annotating individual objects. While evaluating histopathology samples, instead of painstakingly delineating the cancerous tissue, experts usually give a “grade” corresponding to the extent of this tissue [6]. Similarly, in 3D CT lung volumes, it is much easier for the expert to quantitatively estimate the extent

of emphysema instead of performing a complete pixelwise segmentation [7]. In remote sensing, a pixelwise classifier for SAR images was successfully trained from label proportions in low-resolution grid cells [8]. Other applications of LLP include fraud detection [9], video event detection [10], or learning attribute-based representations of images [11].

1.1. Related work

LLP was formulated by Musicant [1] and has been solved by many traditional machine learning approaches [12]. Among support vector machines (SVM) methods [9, 13], Alter- α SVM [14] has received the most attention. It is an example of the Empirical Proportion Risk Minimization (EPRM) framework [15], which learns an instance classifier by minimizing a bag-level loss function defined on the label proportions. The Alter- α SVM algorithm is iterative and alternates between learning the instance classifier and estimation of the instance labels.

Deep LLP (DLLP) [16, 12] was one of the first deep learning LLP methods, and it also uses EPRM. DLLP minimizes a cross-entropy loss on label proportions, which are obtained by averaging the instance label predictions. Other deep learning LLP methods build upon DLLP and use different techniques to improve its robustness. LLP-GAN [17] proposes a generative adversarial network (GAN) where the discriminator is an instance classifier, and the generator attempts to generate images similar to the true images. LLP-VAT [18] adds a consistency term to the proportion loss, which serves as a regularization. An advantage of these methods is that they implicitly support multi-class classification. On the other hand, they require that bags fit into mini-batches, which might not always be feasible (e.g., for 3D images).

1.2. Proposed approach

We focus on the particular case of small bags containing less than $10 \sim 20$ instances. As we will see, this scenario leads to better results by considering all possible configurations consistent with the annotations explicitly, and thus avoiding some of the otherwise necessary approximations, while still having some interesting applications, such as the embryo classification for IVF [2, 3], or analyzing group photos in Section 3.

In particular, we model the instance labels as Bernoulli random variables, whose parameters are calculated by a general

neural network from the instance data. The number of positive instances in each bag is then a Poisson binomial distribution. We propose an EM algorithm to learn the network’s parameters via maximum likelihood estimation. The inner loop of the EM algorithm consists of standard supervised training of the underlying network, interleaved with updating the learning targets using the bag annotations.

The iterative and alternating nature of our algorithm resembles Alter- α SVM. However, our formulation is based on likelihood maximization, not EPRM, and our algorithm allows us to train a deep network which is more powerful than an SVM.

We experimentally compare our approach with two existing LLP methods based on deep learning. The experiments show that our method converges faster and more reliably to solutions that are comparable to or better than the competition.

2. METHODS

2.1. Model and inference

We consider a sample (\mathbf{X}, y) , where $\mathbf{X} = (\mathbf{x}_1, \mathbf{x}_2, \dots, \mathbf{x}_n)$ is a bag of n instances with unknown labels $h_i \in \{0, 1\}$ but known total number of positive labels $y = \sum_{i=1}^n h_i$, $0 \leq y \leq n$. We assume that the example is drawn from a distribution

$$p(\mathbf{X}, y) = P_\theta(y | \mathbf{X})p(\mathbf{X}). \quad (1)$$

We model the conditional probability $P_\theta(y | \mathbf{X})$ parametrized by θ ; $p(\mathbf{X})$ is not modeled as it is not needed for classification.

Let $\mathcal{H} = \{\mathbf{h} \in \{0, 1\}^n \mid \sum_{i=1}^n h_i = y\}$ be the set of all possible instance label configurations \mathbf{h} consistent with the count y . Assuming that the instance label h_i depends only on the instance data \mathbf{x}_i , the conditional probability $P_\theta(y | \mathbf{X})$ is a Poisson binomial distribution

$$P_\theta(y | \mathbf{X}) = \sum_{\mathbf{h} \in \mathcal{H}} P_\theta(\mathbf{h} | \mathbf{X}) \quad (2)$$

$$\text{where } P_\theta(\mathbf{h} | \mathbf{X}) = \prod_{i=1}^n P_\theta(h_i | \mathbf{x}_i). \quad (3)$$

The instance-level probabilities $P_\theta(h_i | \mathbf{x}_i)$ are modeled by a deep network f_θ with weights θ and one sigmoid-activated output,

$$P_\theta(h_i = 1 | \mathbf{x}_i) = f_\theta(\mathbf{x}_i). \quad (4)$$

In this work, \mathbf{x}_i are images but other input types are possible.

At inference time, the predicted label is determined directly by thresholding the deep network’s output,

$$\hat{h}_i = \mathbb{I}[f_\theta(\mathbf{x}_i) \geq \tau], \quad \text{with } \tau = 0.5 \quad (5)$$

2.2. Learning

We are given m training bags $\mathcal{T} = \{(\mathbf{X}_j, y_j)\}_{j=1}^m$. The parameters θ are estimated by maximizing the estimated conditional

log-likelihood

$$\log P(\mathcal{T} | \theta) \approx \mathcal{L}(\theta) = \frac{1}{m} \sum_{j=1}^m \log \sum_{\mathbf{h} \in \mathcal{H}_j} P_\theta(\mathbf{h}_j | \mathbf{X}_j) \quad (6)$$

We follow the EM approach [19], and define

$$\mathcal{L}(\theta, \alpha) = \sum_{j=1}^m \sum_{\mathbf{h} \in \mathcal{H}_j} \alpha_j(\mathbf{h}) \log P_\theta(\mathbf{h} | \mathbf{X}_j) - \alpha_j(\mathbf{h}) \log \alpha_j(\mathbf{h}) \quad (7)$$

$$\text{with } \sum_{\mathbf{h} \in \mathcal{H}_j} \alpha_j(\mathbf{h}) = 1, \quad (8)$$

where $\alpha_j(\mathbf{h}) \geq 0$ are auxiliary variables corresponding to the (yet unknown) posterior probabilities $P(\mathbf{h}_j | \mathbf{X}_j)$. It follows from Jensen’s inequality that $\mathcal{L}(\theta, \alpha) \leq \mathcal{L}(\theta)$. We shall maximize $\mathcal{L}(\theta, \alpha)$ by alternating the following steps:

$$\max_{\alpha} \sum_{j=1}^m \sum_{\mathbf{h} \in \mathcal{H}_j} \alpha_j(\mathbf{h}) \log P_\theta(\mathbf{h} | \mathbf{X}_j) - \alpha_j(\mathbf{h}) \log \alpha_j(\mathbf{h}), \quad (9a)$$

$$\max_{\theta} \sum_{j=1}^m \sum_{\mathbf{h} \in \mathcal{H}_j} \alpha_j(\mathbf{h}) \log P_\theta(\mathbf{h} | \mathbf{X}_j). \quad (9b)$$

2.3. EM steps

In the *expectation* (E) step, the optimization task (9a) is solved w.r.t. the constraints (8). It can be solved independently for each j using a closed-form expression,

$$\alpha_j(\mathbf{h}) = \frac{P_\theta(\mathbf{h} | \mathbf{X}_j)}{\sum_{\mathbf{h}' \in \mathcal{H}_j} P_\theta(\mathbf{h}' | \mathbf{X}_j)}, \quad \text{for } \mathbf{h} \in \mathcal{H}_j. \quad (10)$$

The *maximization* (M) (9b) can be rewritten as

$$\max_{\theta} \sum_{j=1}^m \sum_{i=1}^{n^j} \phi_{ji} \log f_\theta(\mathbf{x}_{ji}) + (1 - \phi_{ji}) \log(1 - f_\theta(\mathbf{x}_{ji})), \quad (11)$$

which corresponds to the binary cross-entropy loss function, so that standard supervised deep learning techniques can be directly employed. The coefficients

$$\phi_{ji} = \sum_{\mathbf{h} \in \mathcal{H}_j} \mathbb{I}[h_{ji} = 1] \alpha_j(\mathbf{h})$$

represent the target instance probabilities $P_\theta(h_{ji} = 1 | \mathbf{X}_j, y_j)$. Since updating the α and ϕ coefficients is not computationally demanding, we do it after each epoch. This turned out to make the algorithm more stable and robust. We stop when the change of \mathcal{L} between iterations drops below $\epsilon = 10^{-4}$.

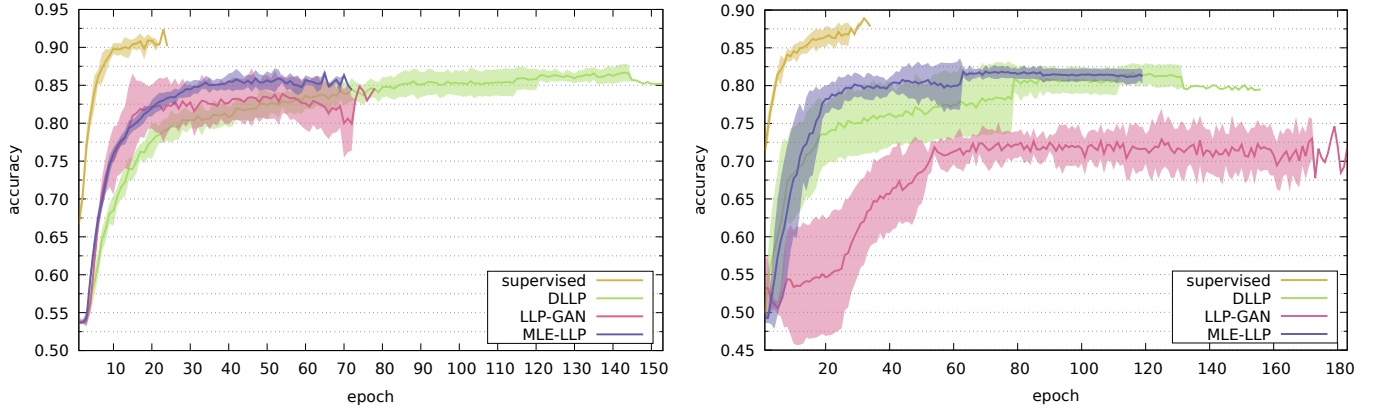


Fig. 1. Learning curve for the group photos (left) and CIFAR (right) dataset. The average test accuracy and the standard deviation is plotted using solid lines and error bands, respectively. One epoch corresponds to one pass of all training data through the newtork for each method.

3. EXPERIMENTS

We compare our method, called MLE-LLP, with a supervised method trained using instance labels, and two existing LLP methods, DLLP [16] and LLP-GAN [17]. All LLP methods were only provided with the number of positive instances in each bag. All experiments were repeated 10 times, randomly splitting the bags into a training (80%) and testing (20%) subsets.

Different backbone network (or discriminator in the case of LLP-GAN) architectures were employed for different datasets, but the generator for LLP-GAN always used the architecture in [17, Table 2 (CIFAR-10)].

The underlying networks of all methods were trained via the Adam [20] optimizer. Image transformations (flipping, blurring, and color adjustments) were applied to prevent over-fitting. The reported results were achieved with the best hyper-parameters discovered through grid-search.

The experiments were implemented using PyTorch 1.7.1 with torchvision 0.8.2 and performed on a server equipped with Intel Xeon Silver 4214R (2.40GHz) and NVIDIA GeForce RTX 2080 Ti.

3.1. Datasets

Two different datasets were used in the experiments. The first dataset, which deals with gender classification, is based on a real-world annotated dataset of family photos [21]. The annotations provide the position, gender, and age category of the faces in each image. We extracted the face regions, rescaled them to 96×120 px, and kept only those of people older than 12 years (see Fig. 2). Faces in one image formed a bag, with images with more than 12 faces omitted, resulting in 1 913 bags of 3 439 and 4 012 male and female instances, respectively. Using the LLP formulation is beneficial in this application, as it is faster to count the number of males/females

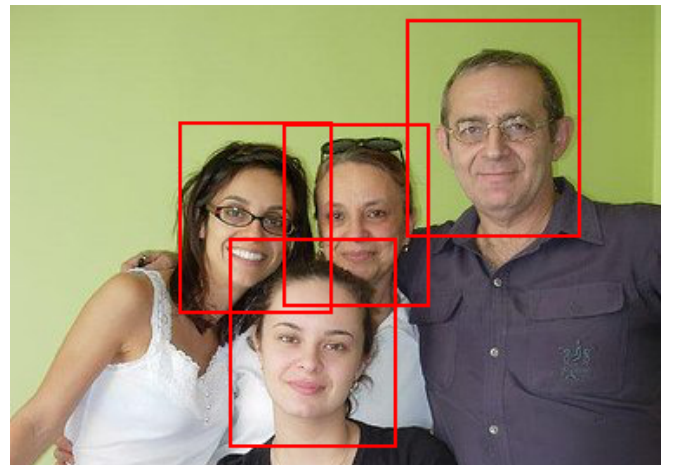


Fig. 2. Example of an image from which a bag of four instances (framed faces) is extracted, three of which are positive (females).

in the photo than manually select the respective faces. ResNet-18 [22] was employed as the backbone network for this dataset.

The second dataset consisted of the *bird* and *cat* classes from the CIFAR-10 [23] dataset, a collection of 32×32 px color images. Bags of uniform random sizes n , $2 \leq n \leq 12$, were constructed by uniform random sampling without replacement. A simpler architecture [17, Table 3 (CIFAR-10)] was used for the backbone networks for this data.

3.2. Convergence speed

The first experiment focused on the convergence speed of the methods. The average epoch time was measured, and the learning curves were plotted for all methods.

All LLP methods achieved slightly lower accuracy than the supervised method (see Fig. 1). Both MLE-LLP and DLLP

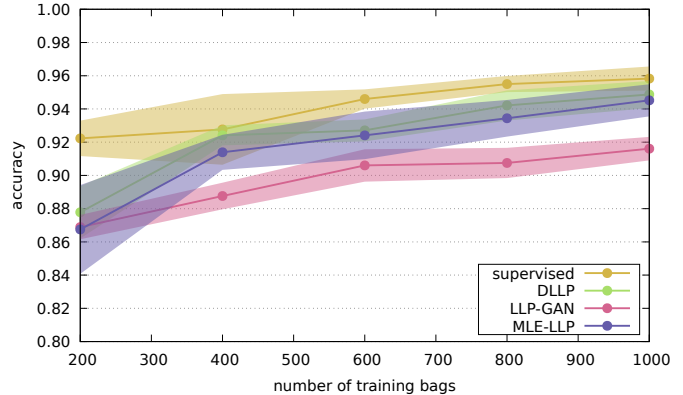
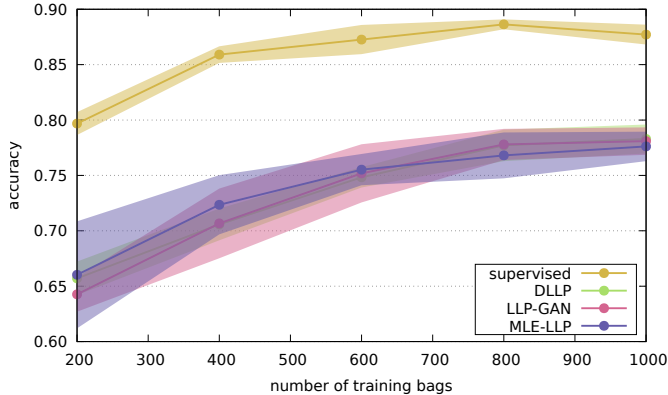


Fig. 3. Dependency of the test accuracy on the number of training bags m for the group photos (left) and CIFAR (right) dataset.

outperformed LLP-GAN. The accuracy of both MLE-LLP and DLLP was comparable, but MLE-LLP converged much faster, reaching the final accuracy in about half the number of epochs. While MLE-LLP and LLP-GAN needed a similar number of epochs for the group photos dataset, LLP-GAN achieved worse performance on the CIFAR dataset, and MLE-LLP was much faster in terms of elapsed time in both cases, as one epoch of LLP-GAN takes several times longer (see Tab. 1). The duration of one epoch of MLE-LLP and DLLP is generally comparable. However, since the CIFAR dataset consists of small images, one epoch of network learning takes only a few seconds, making the relative duration of the E step of the MLE-LLP more noticeable, causing an epoch of MLE-LLP to be slower than DLLP in that case. Note also that the variance of the MLE-LLP during training was smaller than DLLP or LLP-GAN.

3.3. Generalization of LLP methods

The second experiment studied the effect of the size of the training set on the test error. There were five different training sets with $m \in \{200, 400, 600, 800, 1000\}$ bags and a test set with 250 bags for both datasets.

The results (see Fig. 3) again show that the supervised method was always the best, followed by MLE-LLP and DLLP, which were statistically indistinguishable, with the LLP-GAN method being the least accurate. The gap between the supervised and LLP methods is larger for small m and more significant for the group photos. In the case of the CIFAR dataset, the LLP methods approach the performance of supervised learning when enough training data is provided.

4. CONCLUSION

This paper considered learning from label proportions (LLP) when the training dataset consists of small bags. Our MLE-LLP method is general and can be used with any instance classifier. It considers all possible configurations consistent

Table 1. Average epoch durations. For MLE-LLP, the duration includes both the E and M steps.

method	epoch duration [s]	
	group photos	CIFAR
supervised	9.38	7.28
DLLP	16.67	8.16
LLP-GAN	54.36	38.96
MLE-LLP	15.94	11.14

with the annotations, which allows for faster convergence than existing methods based on deep learning. Faster convergence is especially desirable when big datasets consisting of high-dimensional instances are processed. Unlike existing methods, MLE-LLP does not require complete bags to fit into a mini-batch.

Further study of LLP methods is warranted as using LLP allows using bag annotations, which are easier to obtain. While the current LLP methods do not yet achieve the accuracy of fully supervised approaches, we hope that this gap can be decreased in the future.

Acknowledgements

The authors acknowledge the support of the OP VVV funded project “CZ.02.1.01/0.0/0.0/16_019/0000765 Research Center for Informatics” and the Grant Agency of the Czech Technical University in Prague, grant No. SGS20/170/OHK3/3T/13.

5. REFERENCES

- [1] David R. Musicant, Janara M. Christensen, and Jamie F. Olson, “Supervised learning by training on aggregate outputs,” in *Seventh IEEE International Conference on Data Mining*. IEEE, 2007, pp. 252–261.
- [2] Jerónimo Hernández-González, Inaki Inza, et al., “Fitting

the data from embryo implantation prediction: Learning from label proportions,” *Statistical methods in medical research*, vol. 27, no. 4, pp. 1056–1066, 2018.

- [3] Denis Baručić, Jan Kybic, Olga Teplá, Zinovij Topurko, and Irena Kratochvílová, “Automatic evaluation of human oocyte developmental potential from microscopy images,” *arXiv preprint arXiv:2103.00302*, 2021.
- [4] David Habart, Jan Švihlík, et al., “Automated analysis of microscopic images of isolated pancreatic islets,” *Cell Transplantation*, , no. 12, pp. 2145–2156, Dec. 2016.
- [5] Victor Lempitsky and Andrew Zisserman, “Learning to count objects in images,” *Advances in neural information processing systems*, vol. 23, pp. 1324–1332, 2010.
- [6] Peter Bandi, Oscar Geessink, et al., “From detection of individual metastases to classification of lymph node status at the patient level: the camelyon17 challenge,” *IEEE transactions on medical imaging*, vol. 38, no. 2, pp. 550–560, 2018.
- [7] Gerda Bortsova, Florian Dubost, et al., “Deep learning from label proportions for emphysema quantification,” in *International Conference on Medical Image Computing and Computer-Assisted Intervention*. Springer, 2018, pp. 768–776.
- [8] Yongke Ding, Yuanxiang Li, and Wenxian Yu, “Learning from label proportions for sar image classification,” *Eurasip Journal on Advances in Signal Processing*, vol. 2017, no. 1, pp. 1–12, 2017.
- [9] Stefan Rueping, “SVM classifier estimation from group probabilities,” in *Proceedings of the 27th International Conference on International Conference on Machine Learning*, 2010, pp. 911–918.
- [10] Kuan-Ting Lai, Felix X. Yu, et al., “Video event detection by inferring temporal instance labels,” in *Proceedings of the IEEE conference on computer vision and pattern recognition*, 2014, pp. 2243–2250.
- [11] Felix X. Yu, Liangliang Cao, et al., “Modeling attributes from category-attribute proportions,” in *Proceedings of the 22nd ACM international conference on Multimedia*, 2014, pp. 977–980.
- [12] Gabriel Dulac-Arnold, Neil Zeghidour, et al., “Deep multi-class learning from label proportions,” *arXiv preprint arXiv:1905.12909*, 2019.
- [13] Zhensong Chen, Zhiquan Qi, et al., “Learning with label proportions based on nonparallel support vector machines,” *Knowledge-Based Systems*, vol. 119, pp. 126–141, 2017.
- [14] Felix X. Yu, Dong Liu, et al., “ ∞ SVM for learning with label proportions,” in *Proceedings of the 30th International Conference on Machine Learning*, 2013, vol. 28 of *Proceedings of Machine Learning Research*, pp. 504–512, PMLR.
- [15] Felix X. Yu, Krzysztof Choromansky, et al., “On learning from label proportions,” *arXiv preprint arXiv:1402.5902*, 2015.
- [16] Ehsan Mohammady Ardehaly and Aron Culotta, “Co-training for demographic classification using deep learning from label proportions,” in *2017 IEEE International Conference on Data Mining Workshops*. IEEE, 2017, pp. 1017–1024.
- [17] Jiabin Liu, Bo Wang, et al., “Learning from label proportions with generative adversarial networks,” in *Advances in Neural Information Processing Systems*, 2019, pp. 7167–7177.
- [18] Kuen-Han Tsai and Hsuan-Tien Lin, “Learning from label proportions with consistency regularization,” in *Asian Conference on Machine Learning*. PMLR, 2020, pp. 513–528.
- [19] Boris Flach and Vaclav Hlavac, *Computer Vision: A Reference Guide*, chapter Expectation Maximization Algorithm, pp. 265–268, Springer US, Boston, MA, 2014.
- [20] Diederik P. Kingma and Jimmy Ba, “Adam: A method for stochastic optimization,” *arXiv preprint arXiv:1412.6980*, 2014.
- [21] Andrew Gallagher and Tsuhan Chen, “Understanding groups of images of people,” in *IEEE Conference on Computer Vision and Pattern Recognition*, 2009, pp. 256–263.
- [22] Kaiming He, Xiangyu Zhang, et al., “Deep residual learning for image recognition,” in *Proceedings of the IEEE conference on computer vision and pattern recognition*, 2016, pp. 770–778.
- [23] Alex Krizhevsky, “Learning multiple layers of features from tiny images,” Tech. Rep., University of Toronto, 2009, <https://www.cs.toronto.edu/~kriz/learning-features-2009-TR.pdf>, accessed October 2021.